

Input-dependent post-translational control of the reporter output enhances dynamic resolution of mammalian signaling systems

Brianna E.K. Jayanthi^a, Wenting Zhao^b, Laura Segatori^{a,b,c,d,*}

^aSystems, Synthetic, and Physical Biology Graduate Program, Rice University, Houston, TX, United States

Contents

1.	Introduction	2
2.	The NanoDeg platform	5
3.	The NanoDeg as a module for genetic circuits	8
	3.1 Mathematical model of input-dependent NanoDeg reporter circuits	10
	3.2 Design rules of the NanoDeg inverter circuit topology	16
4.	Implementation of a heat shock-inducible NanoDeg inverter circuit	19
	4.1 Tuning the NanoDeg inverter circuit	20
5.	Concluding remarks	23
Ac	knowledgments	23
Re	ferences	23

Abstract

Mammalian cells rely on complex and highly dynamic networks that respond to environmental stimuli and intracellular signals and maintain homeostasis. The use of synthetic orthogonal circuits for detection of dynamic behaviors has been limited by the remarkable stability of conventional reporters. While providing an appealing feature for signal amplification, the long half-life of reporters such as GFP is typically not ideal to measure transient signals and dynamic behaviors. This chapter explores the use of post-translational regulation for the design of input-dependent circuits that produce output signals with enhanced dynamic range and superior dynamic resolution of the input. Specifically, we report the use of the NanoDeg—a bifunctional system that mediates proteasomal degradation of a cellular target with high specificity and control over rate of decay—to achieve input-dependent depletion of a GFP reporter. Feedforward loop

^bDepartment of Chemical and Biomolecular Engineering, Rice University, Houston, TX, United States

^cDepartment of Bioengineering, Rice University, Houston, TX, United States

^dDepartment of Biosciences, Rice University, Houston, TX, United States

^{*}Corresponding author: e-mail address: segatori@rice.edu

topologies were explored and compared to conventional reporters placed directly under control of the input to identify the ideal circuit architecture that allows placing both the GFP output and the GFP-specific NanoDeg under control of a common input and regulate GFP levels not only through input-dependent transcriptional activation but also input-dependent degradation. The circuit design was implemented experimentally by building a heat-sensitive reporter and exploring the design features that result in detection of the cell response with maximal output dynamic range and dynamic resolution of the heat shock. The method reported provides the design rules of a novel synthetic biology module that will be generally useful to build complex genetic networks for enhanced detection of highly dynamic behaviors.

1. Introduction

Green fluorescent protein (GFP) is widely used to quantify gene expression in live cells (March, Rao, & Bentley, 2003; Tsien, 1998). The gene encoding GFP is typically placed under control of a regulated promoter that is sensitive to a specific environmental cue or intracellular signal (Chalfie, Tu, Euskirchen, Ward, & Prasher, 1994; Stearns, Prasher, Tsien, Ward, & Prasher, 1995) and cellular fluorescence monitored to obtain a quantitative measurement of the promoter activity. As most commonly used reporters, whether fluorescent, luminescent, or enzymatic, GFP is a highly stable protein with a reported half-life of ~26h (Corish & Tyler-Smith, 1999), which is generally useful for detection of stimuli of limited intensity. In many cell types, however, GFP half-life is greater than the cell doubling time, resulting in decay of the fluorescence signal that is often governed by dilution due to cell division, rather than by changes in promoter activity, and that fails to provide an accurate measurement of the input dynamics. As a result, GFP is not an ideal reporter for monitoring the response time of transient signals, particularly when focusing on the dynamic behavior associated with removal of the input (Verkhusha et al., 2003; Villaverde & Banga, 2014). Furthermore, ideal reporter systems generate output signals with large dynamic range, which facilitate detection of small, but often biologically relevant changes in gene expression (Korennykh et al., 2009; Kracikova, Akiri, George, Sachidanandam, & Aaronson, 2013; MacKeigan, Murphy, Dimitri, & Blenis, 2005). The high basal expression characteristic of many mammalian signaling networks limits the dynamic range of reporter systems designed to interface with the signaling input (Greber, El-Baba, & Fussenegger, 2008). Moreover, in situations where the basal expression is high, GFP stability can lead to protein crowding that affects the

et al., 2016). This protein crowding phenomenon can lead to inaccurate measurement of the magnitude of change in signal and promoter activity.

To improve the sensitivity of GFP as a reporter of dynamic cellular behaviors, reduced half-life variants such as destabilized GFP variants (dGFP) have been generated by fusing GFP to destabilizing tags or protein signaling domains that confer susceptibility to degradation to the resulting fusion protein (Corish & Tyler-Smith, 1999; Li et al., 1998). As a result, reporter systems based on the reduced half-life dGFP present faster response times (Corish & Tyler-Smith, 1999; Elowitz & Leibier, 2000; Kuhlman, Quintero, & McMahon, 2000; Li et al., 1998; Reya et al., 2003; Tigges, Marquez-Lago, Stelling, & Fussenegger, 2009). The use of unstable GFP variants results in shorter times to reach steady state compared to stable GFP and does not usually affect the signal dynamic range, as the reduction in GFP steady-state levels is independent of the system dynamics (Chen et al., 2018; Del Vecchio & Murray, 2014). Destabilized GFP variants may lead to enhancement of the output dynamic range in cases where the input is applied for a time interval shorter than that needed for GFP levels to reach steady state, but they typically produce low absolute signal outputs (Longo & Hasty, 2006), which are not ideal for sensing applications. These observations point to the need for novel circuit design strategies to enhance dynamic resolution of the input without sacrificing the output dynamic range.

In the present chapter, we investigate the use of input-regulated post-translational control of GFP levels to improve the design of input-dependent circuits. Specifically, we report the use of engineered nanobodies specially designed to control GFP levels through proteasomal degradation. Nanobodies comprise the variable fragment of Camelid single chain antibodies and are the smallest antigen binding fragment (~15 kDa) presenting selectivity and specificity comparable to conventional antibodies (Arbabi Ghahroudi, Desmyter, Wyns, Hamers, & Muyldermans, 1997; Muyldermans, 2013). Due to their small size and high stability, nanobodies present unique properties (Arbabi Ghahroudi et al., 1997; Muyldermans, 2013; Van Der Linden et al., 1999), such as high solubility and low aggregation propensity (Muyldermans, 2013), enhanced tissue penetration and recognition of hidden epitopes (Peng, Lee, Jian, & Yang, 2014), and the ability to recognize conformational epitopes (Domanska et al., 2011; Ghosh, Kumari, Jaiman, & Shukla, 2015) and conformational intermediates (Guilliams et al., 2013).

To build a platform technology for quantitative control over the steadystate levels of a target protein, we built a bifunctional recognition system

(NanoDeg) consisting of a target specific nanobody fused to a degradation signaling unit, the degron, which can be customized with respect to rate and mechanism of degradation and mediates degradation of the nanobody-target complex (Zhao, Pferdehirt, & Segatori, 2018). Nanobodies can be readily obtained from immunized Camelids and engineered through the use of display technologies (Fridy et al., 2014; Fu et al., 2013; Monegal et al., 2009; Moutel et al., 2016; Pardon et al., 2014; Sabir et al., 2014; Schut et al., 2015; Yan, Li, Hu, Ou, & Wan, 2014) to target a variety of seemingly unlimited structures and sequence diversity (Guilliams et al., 2013; Nguyen, Hamers, Wyns, & Muyldermans, 2000; Peng et al., 2014), thus enabling customization of the NanoDeg to target any cellular protein and post-translational modifications. Unlike approaches based on engineering E3 ligases for targeted degradation through the proteasome, which are limited by the structural and functional complexity of this catalytic machinery (Yau & Rape, 2016), degron-mediated depletion relies on a diverse repertoire of sequences for tunable, reversible, and even orthogonal controls over the degradation (Bonger, Chen, Liu, & Wandless, 2011; Bonger, Rakhit, Payumo, Chen, & Wandless, 2014; Chung et al., 2015; Delacour et al., 2015; Holland, Fachinetti, Han, & Cleveland, 2012; Nishimura, Fukagawa, Takisawa, Kakimoto, & Kanemaki, 2009). As a result, the levels of the target protein can be precisely tuned through careful design of the NanoDeg degradationsignaling unit.

Because post-translational control of GFP mediated by the NanoDeg occurs over timescales faster than the transcriptional events mediating GFP expression (Olson & Tabor, 2012), we explored strategies for integration of the NanoDeg into input-dependent circuits with the ultimate goal to attain input-dependent post-translational control of GFP levels. To this end, we explored feedforward loops, which are a class of network motifs frequently observed across biological systems (Mangan & Alon, 2003), that comprise two parallel input-controlled regulation paths. Each feedforward loop affects the output through a direct and an indirect regulation path (Alon, 2006). Feedforward loops can be further classified as coherent or incoherent. In coherent feedforward loops (CFFLs), the direct and indirect regulation paths have the same effect on the output. In incoherent feedforward loops (IFFLs), the two paths are based on opposite regulatory mechanisms, resulting in antagonistic effects on the output (Alon, 2006). Such feedforward motifs constitute the simplest circuit topologies that allow integrating transcriptional and post-translational control of GFP, resulting in direct input-dependent control of GFP and indirect input-dependent

control of the NanoDeg, such that post-translational regulation of the GFP output mediated by the NanoDeg is under control of the input.

Mathematical modeling analyses revealed optimal integration of the NanoDeg can be achieved through a CFFL leading to a NanoDeg Inverter configuration that improves both the output response time and dynamic range. This topology was experimentally implemented by building a cell based sensor of moderate hyperthermia based on a minimal heat-shock promoter derived from the human *hsp70B* gene (Dreano et al., 1986; Huang et al., 2000; Wu, Kingston, & Morimoto, 1986).

2. The NanoDeg platform

We developed a platform technology for targeted, post-translational depletion of cellular proteins based on a bifunctional synthetic protein—the NanoDeg—that provides exquisite control over target identity and rate of depletion. The NanoDeg consists of a molecular recognition unit provided by the nanobody (VHH) and a degradation signaling unit provided by a degron (Zhao et al., 2018). The nanobody mediates recognition of the target with high specificity and selectivity and can be engineered to target virtually any cellular protein (Kolkman & Law, 2010). The degron determines the rate of degradation of the nanobody-target complex and can be customized to convey susceptibility to different pathways of proteasomal degradation and with tunable rate of degradation.

A GFP-specific NanoDeg was built by fusing a GFP-specific nanobody (Caussinus, Kanca, & Affolter, 2012) to either the 16 amino-acid hydrophobic peptide CL1 degron (Gilon, Chomsky, & Kulka, 2000), which is degraded via ubiquitin-dependent proteasomal degradation, or the 37 amino-acid carboxy-terminal sequence of ornithine decarboxylase (ODC degron) (Matsuzawa, Cuddy, Fukushima, & Reed, 2005), which is degraded via ubiquitin-independent proteasomal degradation (Fig. 1A). HEK293T cells stably expressing GFP were transiently transfected with a plasmid encoding a degron-tagged nanobody (VHH_{CL1} and VHH_{ODC}) or the parental nanobody (VHH) and analyzed by flow cytometry 48h post-transfection (Fig. 1B). Cells expressing VHH_{CL1} and VHH_{ODC} displayed a 50% and 65% reduction in GFP fluorescence, respectively, compared to cells expressing the parental VHH. To verify that the reduction in GFP signal is due to proteasomal degradation of GFP in cells expressing the degron-tagged VHHs, we monitored GFP signal upon cell treatment with the proteasome inhibitor MG132 (Kisselev & Goldberg, 2001). Proteasomal inhibition resulted in increase in

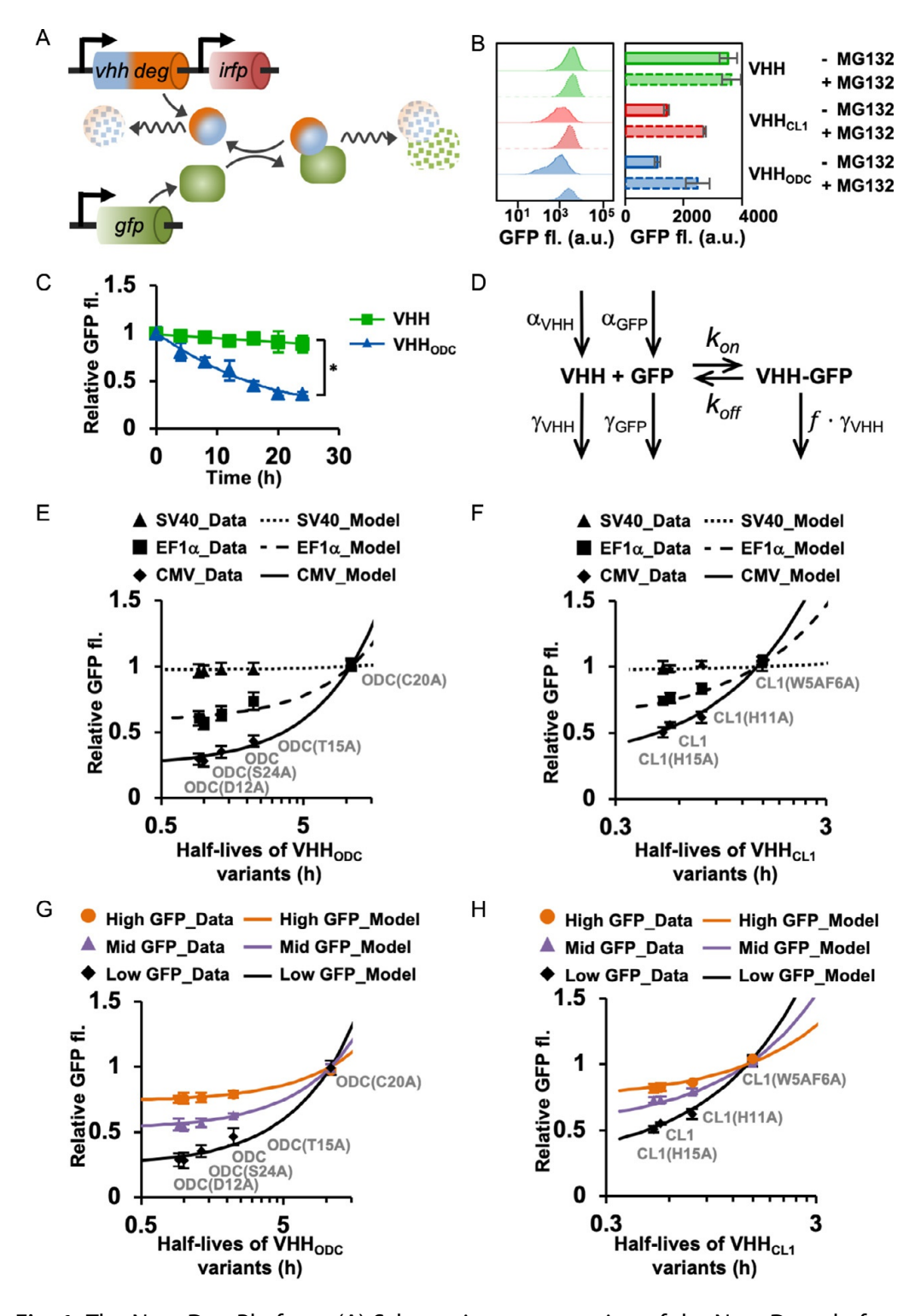


Fig. 1 The NanoDeg Platform. (A) Schematic representation of the NanoDeg platform. (B) GFP signal of stable HEK293T cells expressing GFP transiently transfected for the expression of a VHH variant (VHH, VHH_{CL1}, or VHH_{ODC}) and iRFP (transfection control), untreated or treated with $3\,\mu\text{M}$ MG132 32h post-transfection, and analyzed by flow cytometry 48h post-transfection. Representative flow cytometry histograms showing

the GFP signal of cells expressing VHH_{CL1} and VHH_{ODC} but did not affect that of cells expressing the parental VHH (Fig. 1B, the partial rescue of GFP signal is due to the use of suboptimal MG132 concentration to avoid cell toxicity).

To distinguish between the contribution of GFP synthesis and degradation, we tested the effect of the VHH_{ODC}-based NanoDeg on a photoswitchable GFP variant (PA-GFP) that is photoconverted upon cell exposure to 405 nm light (Patterson, 2002). Cells transfected for the expression of the VHH variants were monitored by flow cytometry to quantify the effect of the NanoDeg on the subset of reporter that is expressed at the time of photoactivation. The fluorescence of cells expressing VHH_{ODC} decreased to half the maximal fluorescence after 16 h from the time of photoactivation, while the fluorescence of cells expressing the parental VHH displayed only 11% decrease after 24 h (Fig. 1C).

GFP intensity of iRFP+ cells (left), and mean GFP fluorescence values of iRFP+ cells (right), reported as mean \pm s.d. (n=3, P<0.005, Student's t-test). (C) Relative GFP fluorescence of stable HEK293T cells expressing photoactivated PA-GFP transiently transfected for expression of a VHH variant (VHH or VHH_{ODC}). Fluorescence of photoactivated cells was measured by flow cytometry and normalized to the GFP fluorescence values of cells at the time of photoactivation. Data are reported as mean \pm s.d. (n=3, *P<0.01, Student's t-test). (D) Mechanism of NanoDeg-mediated degradation of GFP. The reaction is based on synthesis of VHH and GFP (rates α_{VHH} and α_{GFP}), formation of VHH–GFP complex (association rate constant k_{on} and dissociation rate constant k_{off}), degradation of VHH and GFP (rates γ_{VHH} and γ_{GFP}), and degradation of VHH–GFP complex (rate $f \times \gamma_{VHH}$, where f is a degradation coefficient). (E–H) Effect of the rate of VHH synthesis, the rate of GFP synthesis, and the rate of VHH degradation on GFP output. Comparison of modeling results and experimental results of GFP levels as a function of VHH variant half-life. Experimental data are obtained from flow cytometry analyses conducted 48h post-transfection. Relative GFP fluorescence values were calculated by normalizing GFP fluorescence of each sample to that of cells lacking the VHH. Data are reported as mean \pm s.d. (n=3). (E) Relative GFP fluorescence of stable HEK293T cells expressing low GFP levels transiently transfected for expression of VHH_{ODC} variants under the control of the CMV (strong), EF1 α (medium), or SV40 (weak) promoter. (F) Relative GFP fluorescence of stable HEK293T cells expressing low GFP levels transiently transfected for expression of VHH_{CL1} variants under the control of the CMV (strong), EF1 α (medium), or SV40 (weak) promoter. (G) Relative GFP fluorescence of stable HEK293T cell lines expressing high, medium, or low levels of GFP transiently transfected for expression of VHH_{ODC} variants under the control of the CMV promoter. (H) Relative GFP fluorescence of stable HEK293T cell lines expressing high, medium, or low levels of GFP transiently transfected for expression of VHH_{CL1} variants under the control of the CMV promoter. Figure adapted from Zhao, W., Pferdehirt, L., & Segatori, L. (2018). Quantitatively predictable control of cellular protein levels through proteasomal degradation. ACS Synthetic Biology, 7(2), 540-552.

A platform for predictable, quantitative control of the cellular levels of a target protein was generated based on a mathematical model describing the concentration of VHH, GFP and the VHH-GFP complex as dependent on the species-specific rates of synthesis (α) and degradation (γ), and on the rate of dilution due to cell division (μ). The model is based on the assumptions that (1) the rate of degradation of VHH is determined by the specific degron used to build the NanoDeg, (2) VHH binds reversibly to GFP, and (3) the rate of degradation of the VHH-GFP complex is proportional to that of VHH (Fig. 1D). A sensitivity analysis (Zi, 2011) revealed that GFP output is mainly sensitive to the rate of synthesis of VHH (α_{VHH}), the rate of synthesis of GFP (α_{GFP}), and the rate of degradation of VHH (γ_{VHH}). Modulation of the rate of degradation of VHH was achieved experimentally using a series of VHH variants containing mutations in the ODC (Li et al., 1998) and CL1 (Gilon et al., 2000) degron sequences that alter the rate of degradation of the resulting VHH (γ_{VHH}). Modulation of the rate of synthesis of VHH and GFP was achieved by expressing the degron-tagged VHH variants under the CMV, EF1 α , and SV40 promoters to simulate, respectively, high, medium, and low synthesis rate of VHH (α_{VHH}) (Fig. 1E, ODC variants; and Fig. 1F, CL1 variants) (Qin et al., 2010) and in cells stably transfected to express different levels of GFP (Zhao et al., 2018) to simulate high, medium and low synthesis rate of GFP (α_{GFP}) (Fig. 1G, ODC variants; and Fig. 1H, CL1 variants). Flow cytometry results were fitted to the modeling results and validated the predictive value of the mathematical model, thus demonstrating that calibration of VHH synthesis and degradation rates allows modulating GFP depletion with exquisite control.

3. The NanoDeg as a module for genetic circuits

While the NanoDeg platform is potentially useful to investigate the function of any cellular protein through the design of NanoDeg derivatives based on target-specific VHHs and degron with desired degradation rate, the GFP-specific NanoDeg can be specifically used to modulate GFP levels in the context of synthetic networks designed to link GFP output to complex dynamic behaviors. The output signal of gene circuits typically provides an accurate measurement of the input-dependent activation kinetics. The output decay, however, is likely to depend on the reporter's half-life, with stable reporters providing poor indicators of the input decay (March et al., 2003). Reducing the reporter's half-life via genetic engineering partly alleviates

this issue, but also significantly reduces the concentration of the reporter, which may affect detection (Longo & Hasty, 2006). To enhance dynamic control of a GFP reporter and generate a reporter that recapitulates the input dynamics with high fidelity, we integrated the NanoDeg within an input-dependent circuit generating a GFP output signal.

We compared the GFP output of conventional reporters based on expression of GFP (Fig. 2A) or dGFP (Fig. 2B) under the control of the input, to the simplest topologies designed to place the NanoDeg, in addition to GFP, under the control of the input through the use of feedforward loops (Fig. 2C and D). Integrating the NanoDeg under the control of a positive transcriptional regulator that is, in turn, transcriptionally activated by the input results in an IFFL-based circuit (NanoDeg Activator) that mediates input-dependent activation of GFP expression and input-dependent

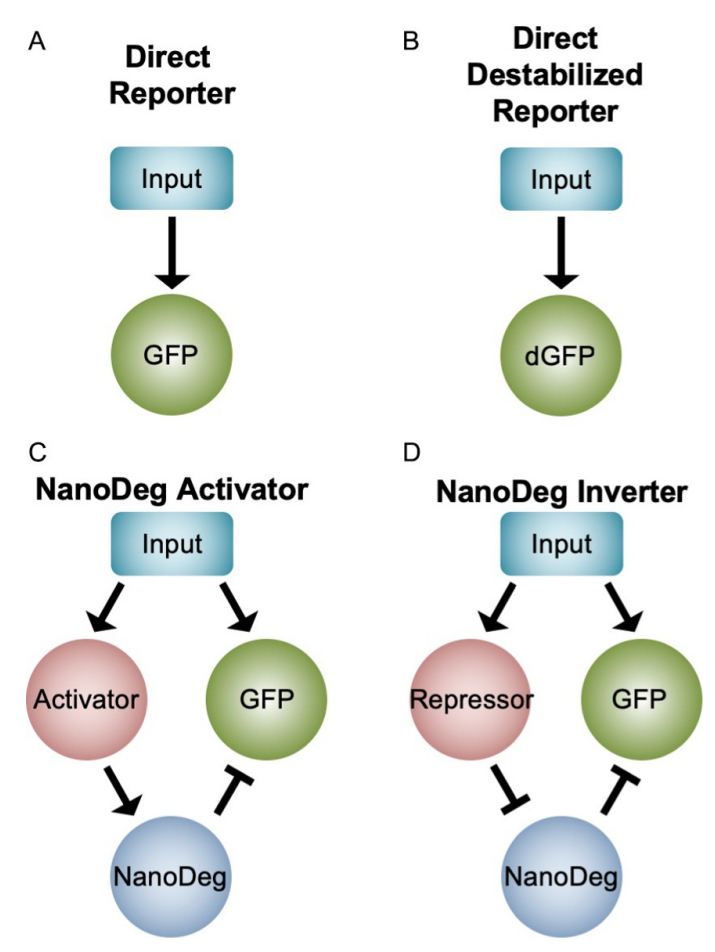


Fig. 2 Schematic representation of genetic network motifs. (A) Direct GFP reporter. (B) Direct destabilized GFP (dGFP) reporter. (C) NanoDeg Activator topology based on the IFFL motif. (D) NanoDeg Inverter topology based on the CFFL motif. Arrows indicate a positive regulation; blunt lines indicate negative regulation.

activation of an activator of the NanoDeg (Fig. 2C). IFFLs are commonly found in biological signaling networks that provide adaptive response (Hornstein & Shomron, 2006; Takeda et al., 2012). The NanoDeg Activator topology could thus be used to engineer circuits with IFFL-like behavior based on post-translational regulation to accurately investigate the adaptive response to biologically relevant stimuli.

The NanoDeg can also be integrated through an inverter topology such that the NanoDeg is under the control of a negative transcriptional regulator that is, in turn, transcriptionally activated by the input. The NanoDeg Inverter results in input-dependent activation of GFP expression and input-dependent activation of a repressor of the NanoDeg, thus generating a CFFL-based circuit that leads to inversion of NanoDeg expression with respect to the input (Fig. 2D). The CFFL of the NanoDeg Inverter topology results in a two-branched input-dependent mechanism of GFP control: direct GFP activation and direct repressor activation followed by indirect NanoDeg repression. As discussed above, the stability of GFP limits its use as a reporter of biological behaviors characterized by fast turnover of relevant components (Mateus & Avery, 2000). The two-branched NanoDeg Inverter topology, on the other hand, is expected to ensure fast turnover of the GFP reporter through NanoDeg-mediated degradation, while maintaining a large dynamic range of the GFP output signal.

3.1 Mathematical model of input-dependent NanoDeg reporter circuits

The NanoDeg-based circuit topologies were first compared by simulating the GFP output of each topology given an input of fixed duration and intensity using a mathematical model based on ordinary differential equations describing the concentration of the species involved (Ingalls, 2014). All species concentration profiles were derived as dependent on rate of synthesis (α), rate of degradation (γ), and rate of cell dilution due to cell growth (μ). The input was introduced using a generalized inducible promoter model with exponential transitions between basal expression (P_{op}) and maximum expression (P_{max}) that follow a rate of activation (β) from basal to maximum activity induced by an input of duration (τ) and a rate of deactivation (β _D) from the maximum to basal activity after removal of the input (Eq. 1). The input was simulated through the activation of an inducible promoter that controls the expression of GFP by affecting the rate of synthesis (α _{GFP}). The direct reporter configurations (Fig. 3A and B) were evaluated by modeling the expression of GFP as the product of the rate of synthesis and a coefficient

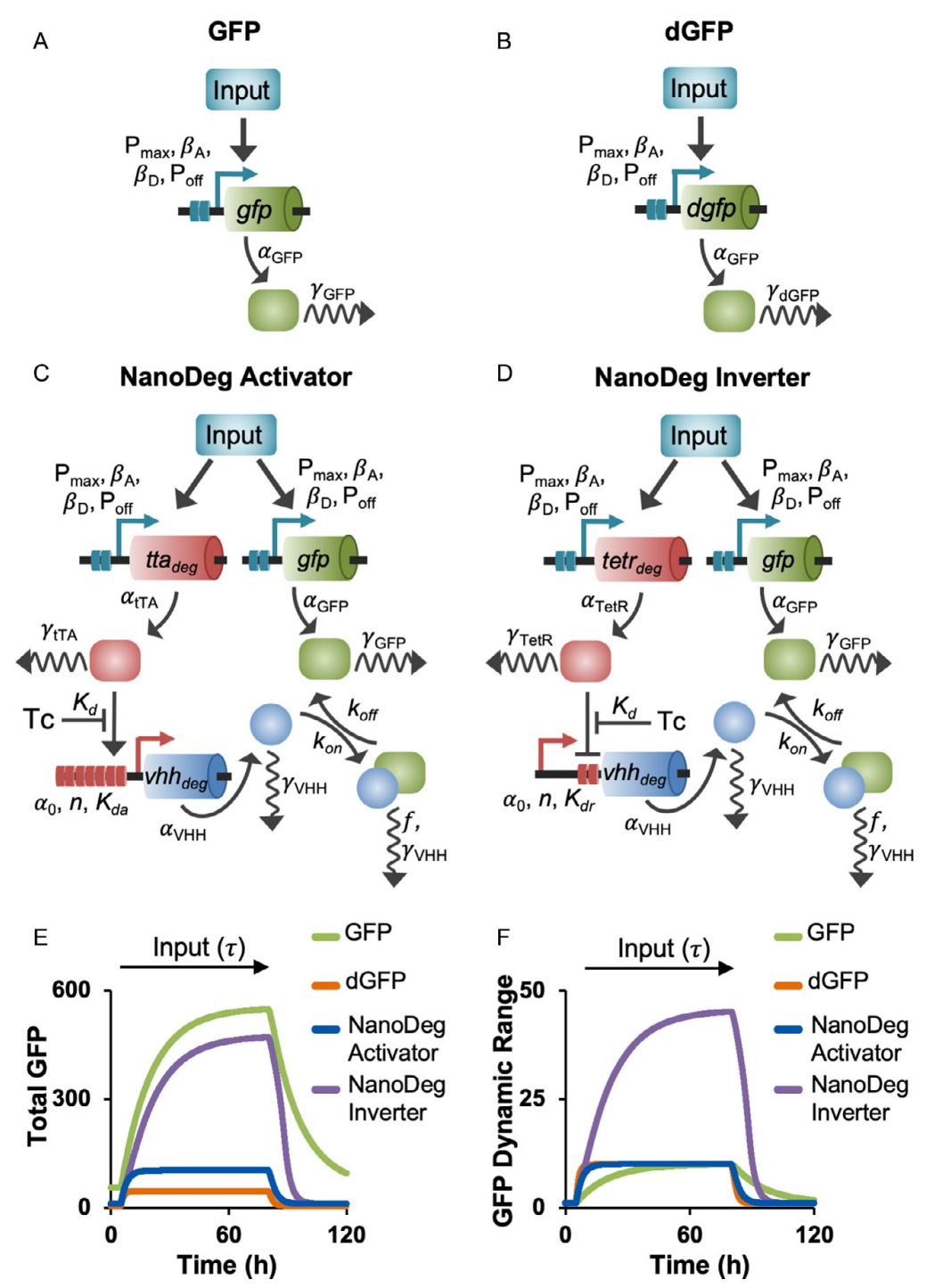


Fig. 3 Mathematical model of the genetic network motifs. (A–D) Diagrams of the models used in this work. The input is modeled assuming an inducible promoter with basal activity (P_{off}), maximal activity (P_{max}), activation rate (β_{A}), and deactivation rate (β_{D}). (A) In the direct GFP reporter, GFP depends on the synthesis rate α_{GFP} and degradation rate γ_{GFP} . (B) In the dGFP reporter, dGFP depends on the synthesis rate α_{GFP} and degradation rate γ_{dGFP} . (C) In the NanoDeg Activator reporter, both GFP and tTA_{deg} are under control of an inducible promoter and depend on the synthesis rates α_{GFP} (Continued)

that accounts for the effect of the inducible promoter ($P_{on} \times \alpha_{GFP}$) (Eq. 2). The direct reporter based on the dGFP was modeled by adjusting GFP degradation rate.

The NanoDeg Activator topology (Fig. 3C) was evaluated by modeling the expression of both GFP and the tetracycline transactivator (tTA) (Gossen & Bujard, 1992) as dependent on their rate of synthesis ($P_{on} \times \alpha_{GFP}$ and $P_{on} \times \alpha_{tTA}$) (Eqs. 3.1 and 3.2), with GFP also being affected by association and dissociation of VHH and GFP governed by the rate constants k_{on} and k_{off} (Eq. 3.4). The expression of the NanoDeg was modeled as dependent on the rate of synthesis regulated by tTA following a Hill Function for an activator with Hill Coefficient (n), rate of synthesis due to leakiness (α_0), and equilibrium dissociation constant of tTA binding to the TO sequence (K_{da}) (Orth, Schnappinger, Hillen, Saenger, & Hinrichs, 2000). The NanoDeg concentration profile is also dependent on the rate of association and dissociation of the VHH-GFP complex (Eq. 3.3).

The NanoDeg Inverter topology (Fig. 3D) was evaluated using a similar approach with the expression of GFP and the tetracycline repressor (TetR) dependent on their rate of synthesis ($P_{on} \times \alpha_{GFP}$ and $P_{on} \times \alpha_{TetR}$) (Eqs. 4.1 and 4.2), and with GFP also affected by association and dissociation of VHH and GFP governed by the rate constants k_{on} and k_{off} (Eq. 4.4).

Fig. 3—Cont'd and α_{tTA} , and degradation rates γ_{tTA} and γ_{GFP} . The expression of the VHH depends on α_0 , tTA_{deq}-TO binding with cooperativity n and equilibrium dissociation constant K_{da} , tTA_{deq}-Tc biding with equilibrium dissociation constant K_d , and degradation with rate γ_{VHH} . The expression of GFP and VHH is also affected by formation of the VHH-GFP complex with association rate constant k_{on} and dissociation rate constant k_{off} and degradation of the VHH-GFP complex with rate $f \times \gamma_{VHH}$. (D) In the NanoDeg Inverter reporter, both GFP and TetR_{deq} are under control of an inducible promoter and depend on the synthesis rates $\alpha_{\rm GFP}$ and $\gamma_{\rm TetR}$, and degradation rates $\gamma_{\rm GFP}$ and $\gamma_{\rm TetR}$. The expression of the VHH depends on α_0 , TetR_{deq}-TO binding with cooperativity n and equilibrium dissociation constant K_{dr} , TetR_{deg}-Tc biding with equilibrium dissociation constant K_{d_l} and degradation with rate γ_{VHH} . The expression of GFP and VHH is also affected by formation and degradation of the VHH-GFP complex as in C. (E) Total GFP output of the topologies modeled as described in A-D simulated using Matlab. GFP expression was simulated for 120 h with a 75 h input duration (τ , indicated with an arrow) starting at time t = 5 h. Steady-state levels of GFP in the absence of the input were used as initial conditions. Total GFP is calculated as either free GFP (for GFP and dGFP), or as the sum of free GFP and VHH-GFP complex (for the NanoDeg Activator and NanoDeg Inverter). (F) GFP dynamic range of the topologies modeled as shown in A–D simulated as descried in E and calculated by normalizing the total GFP values to the total GFP in the absence of the input.

The expression of the NanoDeg was modeled as dependent on the rate of synthesis regulated by TetR following a Hill Function for a repressor with Hill Coefficient (n), rate of synthesis due to leakiness (α_0), and equilibrium dissociation constant of TetR binding to the TO sequence (K_{dr}). The NanoDeg concentration profile is also dependent on the rate of association and dissociation of the VHH-GFP complex (Eq. 4.3).

The NanoDeg-based circuits should be based on short half-life transcriptional regulators (TetR and tTA) to ensure that GFP output dynamics reflects the nature of the input and is not controlled by the half-life of the regulators. The degradation rate of TetR and tTA was thus modeled as the expected degradation rate of ODC(D12A)-tagged TetR and tTA variants (Zhao et al., 2018). Other short half-life components (i.e., the VHH and dGFP) were also modeled as having the degradation rate of an ODC(D12A)-tagged derivative.

$$P_{\text{on}}(t) = \begin{cases} P_{\text{off}} & t < t_{0} \\ P_{\text{off}} + (P_{\text{max}} - P_{\text{off}}) (1 - e^{-\beta_{A}(t - t_{0})}) & t_{0} < t < \tau + t_{0} \\ P_{\text{off}} + (P_{\text{on}}(\tau) - P_{\text{off}}) e^{-\beta_{D}(t - (\tau + t_{0}))}) & t > \tau + t_{0} \end{cases}$$
(1)

$$\frac{d[GFP]}{dt} = \alpha_{GFP} \cdot P_{on}(t) - \left(\gamma_{GFP/dGFP} + \mu\right)[GFP]$$
 (2)

$$\frac{d[GFP]}{dt} = \alpha_{GFP} \cdot P_{on}(t) - (\gamma_{GFP} + \mu)[GFP] - k_{on}[VHH][GFP] + k_{off}[VHH : GFP]$$
(3.1)

$$\frac{d[tTA]}{dt} = \alpha_{tTA} \cdot P_{on}(t) - (\gamma_{tTA} + \mu)[tTA]$$
 (3.2)

$$\frac{d[VHH]}{dt} = \alpha_{VHH} \cdot pTRE \left(\frac{[tTA]^n + \frac{\alpha_0}{\alpha_{VHH}} \cdot K_{da}^n}{K_{da}^n + [tTA]^n} \right) - (\gamma_{VHH} + \mu)[VHH] \\
- k_{on}[VHH][GFP] + k_{off}[VHH : GFP] \tag{3.3}$$

$$\frac{d[VHH:GFP]}{dt} = k_{on}[VHH][GFP] - k_{off}[VHH:GFP] - (f \cdot \gamma_{VHH} + \mu)[VHH:GFP]$$
(3.4)

$$\frac{d[GFP]}{dt} = \alpha_{GFP} \cdot P_{on}(t) - (\gamma_{GFP} + \mu)[GFP]
- k_{on}[VHH][GFP] + k_{off}[VHH : GFP]$$
(4.1)

$$\frac{d[TetR]}{dt} = \alpha_{TetR} \cdot P_{on}(t) - (\gamma_{TetR} + \mu)[TetR] \qquad (4.2)$$

$$\frac{d[VHH]}{dt} = \alpha_{VHH} \cdot pTO \left(\frac{1 + \frac{\alpha_0}{\alpha_{VHH}} \left(\frac{[TetR]}{K_{dr}} \right)^n}{1 + \left(\frac{[TetR]}{K_{dr}} \right)^n} \right)$$

$$- (\gamma_{VHH} + \mu)[VHH]$$

$$- k_{on}[VHH][GFP] + k_{off}[VHH : GFP]$$

$$\frac{d[VHH : GFP]}{dt} = k_{on}[VHH][GFP] - k_{off}[VHH : GFP]$$

$$- (f \cdot \gamma_{VHH} + \mu)[VHH : GFP] \qquad (4.4)$$

The basal steady-state levels of GFP (in the absence of input) were used as initial conditions for simulations of total GFP levels upon introduction of the input, which were quantified as free GFP for the direct reporters and as the sum of free GFP and VHH-GFP complex concentrations for NanoDeg Inverter and NanoDeg Activator topologies. All topologies were simulated by evaluating GFP output as a function of time with the input introduced at $t=5\,\mathrm{h}$ for $\tau=75\,\mathrm{h}$, and using the parameters listed in Table 1 (Fig. 3E). GFP dynamic range was calculated by normalizing the GFP levels at each time point to the GFP levels immediately before introduction of the input for each circuit (Fig. 3F).

As expected, the GFP signal of the reporter based on dGFP presents improved dynamic resolution of the input decay and reduced absolute output signal compared to the reporter based on stable GFP. Specifically, the dGFP based reporter displays a six-fold reduction in the response time (defined as the time of decay to half of the maximum GFP levels) at the expense of a marked reduction in absolute GFP levels (Fig. 3E). The dynamic range did not differ significantly between the two reporters as it arises from a proportional reduction in both induced and non-induced (basal) levels of dGFP compared to stable GFP (Fig. 3F).

The NanoDeg Activator and NanoDeg Inverter topologies are designed to achieve input-mediated control of GFP at the post-translational level: input-induced activation of GFP degradation through the NanoDeg Activator topology and input-induced repression of GFP degradation through the NanoDeg Inverter topology. In the NanoDeg Activator configuration, activation of NanoDeg-mediated degradation results in dramatic reduction in GFP steady-state levels compared to the direct GFP reporter (Fig. 3E).

	odel parameters used in this s Description	study. Value	Source	
$P_{ m max}$	Inducible promoter maximum activity	36	Literature Data ^{a,b}	
$\overline{P_{o\!f\!f}}$	Inducible promoter basal activity	3.6	This work ^c	
$oldsymbol{eta}_A$	Inducible promoter activation rate	$5 \mathrm{nMh}^{-1}$	Arbitrary value	
$oldsymbol{eta}_D$	Inducible promoter deactivation rate	$1 \mathrm{nM}\mathrm{h}^{-1}$	Arbitrary value	
P_{on}	Inducible promoter activity at time <i>t</i>	Variable	This work	
$\overline{lpha_{GFP}}$	GFP synthesis rate	$1 \mathrm{nM}\mathrm{h}^{-1}$	Assuming synthesis rate is equal to P_{on} (Eq. 1)	
γ_{GFP}	GFP degradation rate	0.0267h^{-1}	Literature Data ^b	
μ	Cell dilution rate	$0.0385\mathrm{h^{-1}}$	Literature Data ^b	
γ_{dGFP}	dGFP degradation rate	$0.7534\mathrm{h^{-1}}$	Literature Data ^d	
$\overline{lpha_{V\!H\!H}}$	VHH synthesis rate	$281 \text{nM} \text{h}^{-1}$	Literature Data ^d	
ү үнн	VHH degradation rate	$0.7534\mathrm{h}^{-1}$	Literature Data ^d	
kon	VHH-GFP association rate constant	$2.7648 \text{nM}^{-1} \text{h}^{-1}$	Literature Data ^d	
k_{off}	VHH-GFP dissociation rate constant	$0.6264\mathrm{h}^{-1}$	Literature Data ^d	
f	Degradation coefficient of VHH _{ODC} -GFP complex	0.414	Literature Data ^d	
$\overline{lpha_{tTA}}$	tTA synthesis rate	$1 \mathrm{nM}\mathrm{h}^{-1}$	Assuming synthesis rate is equal to P_{on} (Eq. 1)	
$\overline{\alpha_{0-tTA}}$	Leakiness of inducible VHH	$5 \mathrm{nM}\mathrm{h}^{-1}$	Literature Data ^b	
n_{tTA}	Cooperativity of tTA-TO binding	2	Literature Data ^b	
K_{da}	tTA-TO equilibrium dissociation constant	3.0 nM	Literature Data ^b	
· · · · · · · · · · · · · · · · · · ·		·		

Continued

Parameter	Description	Value	Source
$\overline{lpha_{TetR}}$	TetR synthesis rate	$1\mathrm{nM}\mathrm{h}^{-1}$	Assuming synthesis rate is equal to P_{on} (Eq. 1)
$\overline{lpha_{ extit{0-TetR}}}$	Leakiness of repressible VHH	$5\mathrm{nMh}^{-1}$	Literature Data ^b
n_{TetR}	Cooperativity of TetR- TO binding	2	Literature Data ^b
K_{dr}	TetR-TO equilibrium dissociation constant	3.0 nM	Literature Data ^b

Table 1 Model parameters used in this study.—cont'd

Because the basal GFP levels are also reduced, the dynamic range of GFP output upon introduction of the input is comparable to that of the direct reporter. The response time of the NanoDeg Activator circuit, however, is significantly improved compared to the direct GFP reporter due to post-translational depletion of GFP resulting in GFP decay similar to that of the dGFP reporter (Fig. 3F).

Repression of NanoDeg-mediated degradation in the NanoDeg Inverter configuration results in GFP steady-state levels comparable to those of the direct GFP reporter upon induction of the system, and reduced GFP levels under basal conditions and upon removal of the input (Fig. 3E), which improves the output dynamic range dramatically (Fig. 3F). Moreover, NanoDegmediated degradation also improves the output response time due to post-translation depletion of GFP (Fig. 3E and F).

In summary, the NanoDeg Inverter configuration provides a topology that enhances the dynamic range of an input-dependent output and dynamic resolution of the input.

3.2 Design rules of the NanoDeg inverter circuit topology

To define design rules of the NanoDeg Inverter topology, we performed a global sensitivity analysis and quantified the parameter sensitivities (Fig. 4A). The global sensitivity analysis allows characterizing the response of the GFP output to perturbations in the circuit parameters, ultimately informing design optimization. To this end, the model was simulated in the COPASI

^aGerner et al. (2000).

^bZhao, Bonem, McWhite, Silberg, and Segatori (2014).

^cValue estimated from HEK293T cells transiently transfected for expression of GFP under control of the *hsp70B* promoter.

^dZhao et al. (2018).

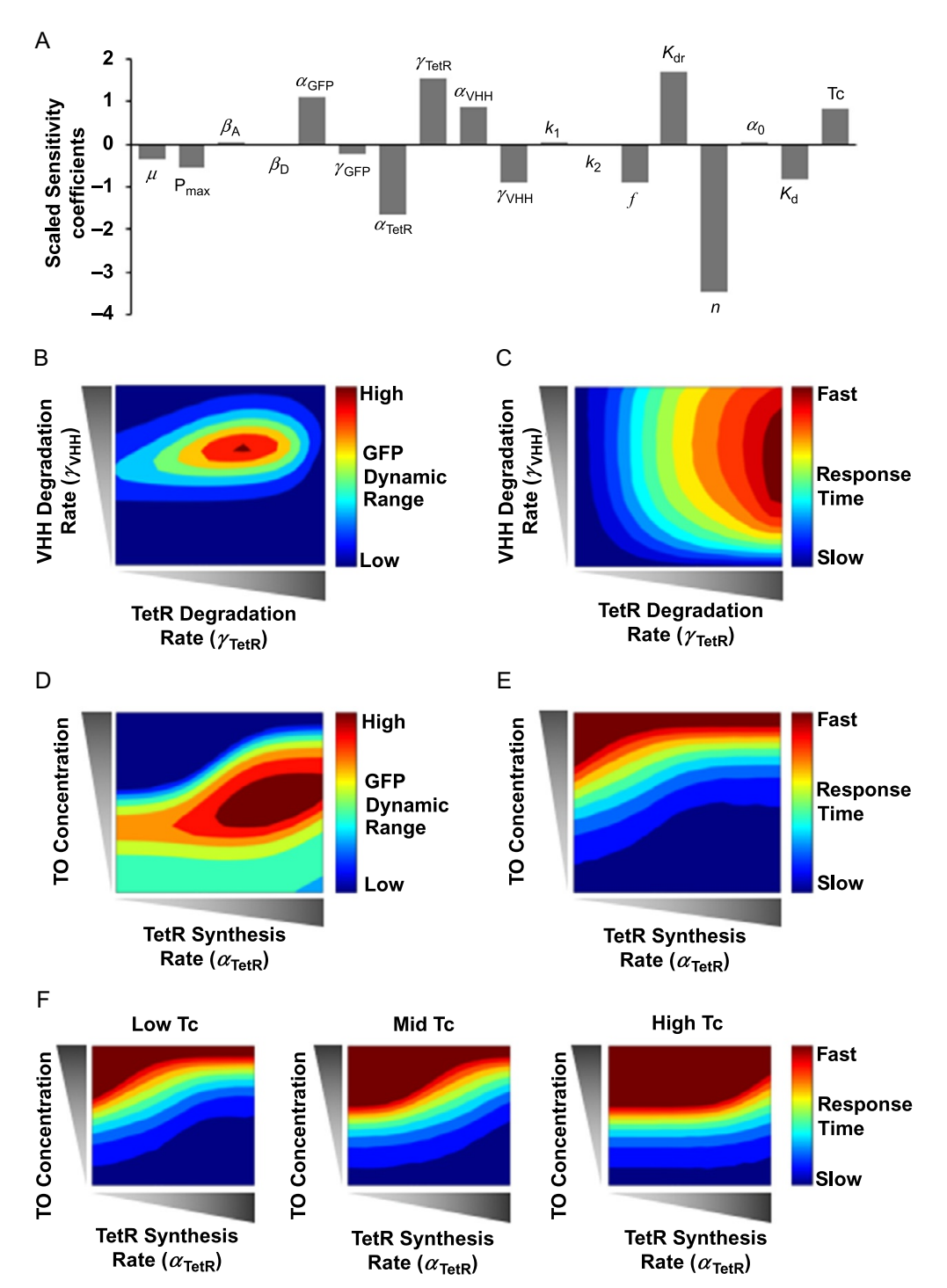


Fig. 4 Design Rules of the NanoDeg Inverter Topology. (A) Sensitivity of GFP output to perturbations in the NanoDeg Inverter parameters. The sensitivity analysis was performed using COPASI software with default parameter step size. (B–F) GFP levels of the NanoDeg Inverter simulated for 120 h. The input is introduced at time $t=5\,\mathrm{h}$ for 75 h. (B) GFP Dynamic Range as a function of NanoDeg degradation rate (γ_{VHH}) and TetR degradation rate (γ_{TetR}). GFP Dynamic Range was calculated by normalizing the total GFP levels upon exposure to the input to the total GFP levels prior to exposure to the input. (C) GFP response time as a function of NanoDeg degradation rate (γ_{VHH}) and TetR degradation rate (γ_{TetR}). The response time was calculated as the time to decay to half of the maximum total GFP value. (D) GFP Dynamic Range as a function of the TO concentration (which is proportional to the maximum α_{VHH}) and TetR synthesis rate (α_{TetR}). (E) GFP response time as a function of TO concentration and TetR synthesis rate (α_{TetR}). (F) GFP response time as a function of TO concentration and TetR synthesis rate (α_{TetR}) in the presence of high (10^{-7} nM), mid (10^{-8} nM), and low (10^{-9} nM) Tc.

software (Hoops et al., 2006). Parameters identified based on the sensitivity analysis that could be actually altered experimentally, such as tetracycline (Tc) dosage, or through alterations in the circuit design, such as the NanoDeg and TetR synthesis and degradation rates, were further explored. Simulations of the NanoDeg Inverter circuit were conducted to characterize the dynamic range (total GFP normalized to total GFP in the absence of the input) and the response time (time to decay to half of the maximum GFP levels) in response to alterations in Tc dosage, the NanoDeg degradation rate, TetR synthesis and degradation rates, and the concentration of TO sequences (Fig. 4B-F). Analysis of GFP dynamic range as a function of the rates of degradation of VHH and TetR (γ_{VHH} and γ_{TetR}) revealed the design constrains of the NanoDeg Inverter circuit (Fig. 4B). There appear to be lower and upper thresholds of γ_{VHH} , beyond which γ_{TetR} does not affect the output dynamic range and an optimum γ_{TetR} within these limits. Low γ_{TetR} values are expected to result in repression of the NanoDeg, effectively generating a circuit regulated by TetR half-life, and resulting in a behavior that approaches that of the direct GFP reporter. Large $\gamma_{\rm TetR}$ values, on the other hand, are expected to eliminate input-mediated control of NanoDeg expression, effectively placing GFP output under control of a constitutively expressed NanoDeg and resulting in a behavior that approaches that of the direct dGFP reporter (Fig. 4B).

Analysis of GFP response time as a function of the rates of degradation of VHH and TetR (γ_{VHH} and γ_{TetR}) confirmed that the response time is largely affected by γ_{TetR} (Fig. 4C), which is in agreement with the notion that rapid degradation of TetR upon removal of the input results in rapid expression of the NanoDeg and depletion of residual GFP. These results point to a potential tradeoff between response time and dynamic range of the system (Fig. 4B and C) and the need to carefully tune γ_{TetR} and γ_{VHH} to avoid deregulated depletion of GFP, which enhances the output response time at the expense of the output dynamic range.

We next studied the response of the NanoDeg Inverter circuit to alterations in the rate of TetR synthesis (α_{TetR}) and the concentration of DNA operator (TO concentration), which is proportional to the maximum NanoDeg synthesis rate (Fig. 4D). For a given value of α_{TetR} , the dynamic range increases as a function of TO concentration until a TO concentration that exceeds the TetR capacity to repress the NanoDeg, effectively approaching the behavior of the direct dGFP reporter. The threshold of TO concentration increases as α_{TetR} increases with a characteristic sigmoidal behavior. These modeling results also predict the conditions to maximize

GFP dynamic range based on the optimal TO concentration for expression of the NanoDeg in the absence of the input and optimal α_{TetR} for repression of the NanoDeg in the presence of the input.

The response time is also affected by the TO concentration and TetR synthesis rate (Fig. 4E). Generally speaking, the response time increases as a function of TO concentration due to incomplete repression of NanoDeg expression, with the lower limit of TO concentration increasing as a function of $\alpha_{\rm TetR}$, reflecting the increase in TetR levels available for TO repression. These results point to a design tradeoff with respect to TO concentration and TetR synthesis rate and to the need to carefully tune TO concentration and $\alpha_{\rm TetR}$ to ensure depletion of GFP levels in the absence of the input and efficient repression of the NanoDeg in the presence of the input.

Tc dosage affects the binding equilibrium of TetR and the TO sequence (Orth et al., 2000). Tc dosage is thus expected to cause an apparent reduction in TetR synthesis rate, resulting in modulation of the GFP response time for a given TO concentration. Modeling prediction of the GFP response time as a function of TO concentration and TetR synthesis rate and in the presence of increasing Tc concertation confirmed that Tc dosage increases the output response time (Fig. 4F).



4. Implementation of a heat shock-inducible NanoDeg inverter circuit

The NanoDeg Inverter circuit was tested experimentally in cells expressing a GFP reporter of heat shock. HEK293T cells were transduced for the expression of GFP under control of the minimal *hsp70B* promoter (Dreano et al., 1986; Huang et al., 2000; Wu et al., 1986) and a stable monoclonal population selected (HS-GFP cells). To verify that the NanoDeg degradation rate affects GFP response time, the decay of GFP signal was tested in the context of a series of NanoDeg Inverter circuits based on NanoDeg variants presenting mutations in the ODC tag expected to affect the NanoDeg half-life, namely ODC (1.3h), ODC(C20A) (10.8h) and ODC(D12A) (0.9 h) (Zhao et al., 2018). HS-GFP cells were co-transfected for the expression of (i) TetR_{ODC(D12A)} (a TetR variant expected to display fast degradation rate (Zhao et al., 2018) selected to ensure TetR half-life does not affect the output dynamics) under the control of the minimal *hsp70B* promoter and linked to the expression of a near-infrared fluorescent protein (eqFP650) (Shcherbo et al., 2010) through an internal ribosome entry site (IRES)

(Ghattas, Sanes, & Majors, 1991), and (ii) a NanoDeg variant or the parental VHH under the control of the TetR regulated CMV promoter containing two repeats of the TO sequence downstream of the TATA box (CMV/TO) (Yao et al., 1998). Cells were transfected with plasmids for the expression of TetR and the NanoDeg in a 10:1 ratio and exposed to the input (43°C for 90 min 24 h after transfection). GFP fluorescence of eqFP650 fluorescent cells was recorded as a function of time. GFP decay rate, quantified between 12 h and 18 h post-induction, was found to correlate with the degradation rate of the NanoDeg (Fig. 5A). These results confirm that the NanoDeg degradation rate affects the GFP output of the NanoDeg Inverter circuit and led to the generation of a stable cell line expressing the NanoDeg based on ODC(D12A) to implement the complete heat-shock sensitive NanoDeg Inverter circuit.

A stable HEK293T cell line expressing GFP and a degron-tagged TetR variant under the control of a heat-shock sensitive promoter and the NanoDeg under the control of TetR was generated by first transducing HS-GFP cells to integrate a cassette containing the gene encoding VHH_{ODC(D12A)}, an IRES, and the gene encoding the infrared fluorescent protein (iRFP) (Filonov et al., 2011) under control of the CMV/TO promoter. Transduced cells were subsequently transduced for the expression of TetR_{ODC(D12A)}-IRES-eqFP650 under control of the minimal hsp70B promoter. The resulting polyclonal population was analyzed by FACS to isolate single cells exhibiting high eqFP650 signal (corresponding to high TetR_{ODC(D12A} expression) and high iRFP signal (corresponding to high VHH_{ODC(D12A)} expression). Monoclonal populations were further screened by flow cytometry to select a monoclonal stable cell line displaying maximal GFP dynamic range (compared to the parental HS-GFP cell line not containing TetR and the NanoDeg) and sensitivity to Tc, which is expected to affect the expression of the NanoDeg and thus degradation of GFP. The resulting monoclonal cell line containing the complete NanoDeg Inverter circuit was selected for further experiments. A monoclonal cell line stably expressing dGFP (GFP_{ODC(D12A)}) under the control of the minimal hsp70B promoter was also generated for comparison.

4.1 Tuning the NanoDeg inverter circuit

To identify the Tc dosage that maximizes the circuit sensitivity to heat shock, we measured the GFP output of HEK293T cells expressing the NanoDeg Inverter circuit as a function of Tc concentration in the culturing

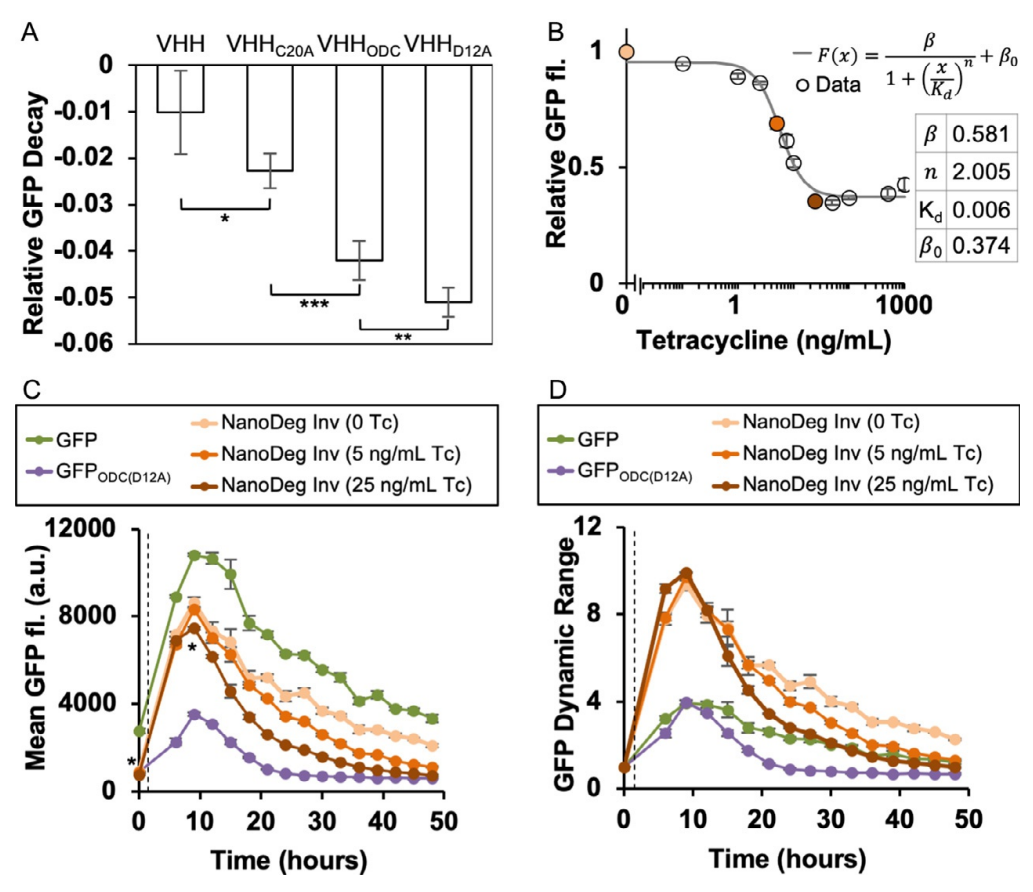


Fig. 5 Implementation of a heat shock-inducible NanoDeg Inverter circuit. (A) GFP output of stable HEK293T cells expressing GFP under control of the minimal hsp70B promoter transiently transfected with TetR_{ODC(D12A)}-IRES-eqFP650 under control of the minimal hsp70B promoter and VHH variants under control of the CMV/TO promoter. Cells were exposed to heat-shock (90 min at 43°C) 24 h post-transfection. Transfected cells were analyzed by flow cytometry at 12h, 15h, and 18h post-heat shock. Relative GFP values were calculated by normalizing the mean GFP values of egFP650+ and GFP+ cells exposed to heat shock to the mean GFP values of untreated cells. The relative GFP decay was obtained by calculating the slope of the relative GFP values between 12 h and 18h. Data are reported as mean \pm s.d. (n = 5, *P < 0.05, **P < 0.01, ***P < 0.0001, Student's t-test). (B) GFP fluorescence of stable HEK293T cells expressing the heat sensitive NanoDeg Inverter circuit as a function of Tc dosage. Cells were treated with Tc for 24 h prior to heat-shock treatment (90 min at 43°C). GFP fluorescence was measured by flow cytometry 24h post-heat shock. Relative GFP values, calculated by normalizing the GFP fluorescence of Tc-treated cells to that of untreated cells, were fit to a Hill function using Matlab nonlinear least-squares solver. Data are reported as mean \pm s.d. (n = 3). (C) GFP output of stable HEK293T cells expressing GFP or GFP_{ODC(D12A)} under control of the minimal hsp70B promoter, or stable HEK293T cells expressing the heat sensitive NanoDeg Inverter circuit. Cells were treated with Tc for 24h prior to exposure to heat-shock (90 min at 43°C, dashed line). Flow cytometry measurements were conducted immediately prior to heat-shock (t=0h) and every 3h between 6 and 48h post-heat shock. Data are reported as mean \pm s.d. (n=3, *P<0.001, Student's t-test). (D) GFP dynamic range calculated by normalizing the mean GFP values of cells treated as in (C) to the mean GFP values prior to heat shock.

medium. Cells were exposed to Tc for 24h, heat shocked at 43°C for 90 min (Dreano et al., 1986), and analyzed by flow cytometry 24h from the initial time of exposure to heat shock to quantify GFP fluorescence (Fig. 5B). The experimental data were fitted to a Hill function for a repressor with basal expression (F(x)) using the least-squares method. Noticeably, the resulting Hill coefficient (n) is approximately 2, as expected for a dimeric repressor (Hillen, Gatz, Altschmied, Schollmeier, & Meier, 1983).

Cells expressing heat shock sensitive GFP, heat shock sensitive destabilized GFP_{ODC(D12A)}, or the heat shock sensitive NanoDeg Inverter circuit (5×10⁴ cells, 24-well plates) were treated with representative concentrations of Tc (0, 5, and 25 ng/mL) for 24 h prior to heat shock (43°C for 90 min). Flow cytometry measurements of GFP output as a function of time were recorded for 48 h from the initial time of exposure to the input (Fig. 5C and D). The maximum GFP output was reached 9 h post-induction in all circuits and independently of the Tc dosage. The response time of the NanoDeg Inverter in the absence of Tc was similar to that of the GFP-based direct reporter (~15h). This result is expected when the concentration of TetR is in large excess compared to that of the TO sequence (see Fig. 4D and E) and depletion of TetR to an extent that results in activation of NanoDeg synthesis is slower than the rate of degradation of GFP.

Addition of Tc is expected to decrease the pool of TetR that can bind to the TO sequence, resulting in rapid activation of NanoDeg expression upon removal of the input. Culturing cells expressing the NanoDeg Inverter circuit in the presence of 5 ng/mL Tc decreases the response time to approximately 12h and does not significantly reduce the basal (0h) or maximum (9h) GFP fluorescence. Addition of higher Tc concentration (25 ng/mL), however, does significantly reduce both the basal and maximum GFP fluorescence (Fig. 5C, *P<0.001, Student's t-test). Treatment with 25 ng/mL Tc also further enhances the response time to approximately 9 h, which is the same response time measured for cells expressing GFP_{ODC(D12A)}. GFP dynamic range values were obtained by normalizing the mean GFP fluorescence of each sample to the GFP signal of uninduced cells for each topology and Tc condition (Fig. 5D). The GFP output dynamic range of cells expressing the heat sensitive NanoDeg Inverter was found to be three-fold higher than that of cells expressing the direct (GFP) and destabilized (GFP_{ODC(D12A)}) reporters, regardless of Tc dosage. In addition, the response time of cells expressing the NanoDeg Inverter circuit exposed to Tc (25 ng/mL) (~9h) was found to be considerably shorter than that of cells expressing the direct GFP reporter (~15h) due to the rapid depletion of GFP mediated by the NanoDeg (Fig. 5D). These results demonstrate that the NanoDeg Inverter circuit provides a robust topology for monitoring signal dynamics and can be experimentally tuned to enhance the dynamic resolution of the input.

5. Concluding remarks

In this chapter, we report the development of a platform technology (NanoDeg) to achieve quantitative and predictable control of the cellular levels of a target protein (Zhao et al., 2018) and the implementation of this technology to build reporter systems for detection of dynamic behaviors through input-dependent degradation of the reporter output. We investigate the design rules for integrating the NanoDeg within an inputdependent genetic circuit to achieve enhanced output dynamic range and dynamic resolution of the input, which are particularly appealing features for detection of transient behaviors that are often biologically relevant. The NanoDeg Inverter circuit described in the present study provides the first report of transcriptional and post-translational regulation combined in a synthetic coherent feedforward loop topology. Moreover, the NanoDeg Inverter circuit responds to endogenous inputs with a tunable output. This feature is particularly important for connecting individual modules to generate genetic circuits of greater complexity (Kobayashi et al., 2004; Slusarczyk, Lin, & Weiss, 2012) and represents a currently unmet goal in the field of synthetic biology.

Acknowledgments

This work was funded by The National Science Foundation (CBET-1805317 and CBET-1615562) and the Welch Foundation (C-1824). This project was supported by the Cytometry and Cell Sorting Core at Baylor College of Medicine with funding from the NIH (CA125123 and RR024574) and the expert assistance of Joel M. Sederstrom.

References

Alon, U. (2006). An introduction to systems biology: Design principles of biological circuits. Boca Raton, FL: Chapman and Hall/CRC.

Arbabi Ghahroudi, M., Desmyter, A., Wyns, L., Hamers, R., & Muyldermans, S. (1997). Selection and identification of single domain antibody fragments from camel heavychain antibodies. *FEBS Letters*, 414(3), 521–526.

Bonger, K. M., Chen, L. C., Liu, C. W., & Wandless, T. J. (2011). Small-molecule displacement of a cryptic degron causes conditional protein degradation. *Nature Chemical Biology*, 7(8), 531.

Bonger, K. M., Rakhit, R., Payumo, A. Y., Chen, J. K., & Wandless, T. J. (2014). General method for regulating protein stability with light. *ACS Chemical Biology*, 9(1), 111–115.

- Caussinus, E., Kanca, O., & Affolter, M. (2012). Fluorescent fusion protein knockout mediated by anti-GFP nanobody. *Nature Structural and Molecular Biology*, 19(1), 117–122.
- Chalfie, M., Tu, Y., Euskirchen, G., Ward, W., & Prasher, D. (1994). Green fluorescent protein as a marker for gene expression. *Science*, 263(5148), 802–805.
- Chen, Y., Ho, J. M. L., Shis, D. L., Gupta, C., Long, J., Wagner, D. S., et al. (2018). Tuning the dynamic range of bacterial promoters regulated by ligand-inducible transcription factors. *Nature Communications*, 9(1), 1–8.
- Chung, H. K., Jacobs, C. L., Huo, Y., Yang, J., Krumm, S. A., Plemper, R. K., et al. (2015). Tunable and reversible drug control of protein production via a self-excising degron. *Nature Chemical Biology*, 11(9), 713.
- Corish, P., & Tyler-Smith, C. (1999). Attenuation of green fluorescent protein half-life in mammalian cells. *Protein Engineering, Design and Selection*, 12(12), 1035–1040.
- Del Vecchio, D., & Murray, R. M. (2014). *Biomolecular feedback systems*. Princeton, NJ: Princeton University Press.
- Delacour, Q., Li, C., Plamont, M. A., Billon-Denis, E., Aujard, I., Le Saux, T., et al. (2015). Light-activated proteolysis for the spatiotemporal control of proteins. *ACS Chemical Biology*, 10(7), 1643–1647.
- Domanska, K., Vanderhaegen, S., Srinivasan, V., Pardon, E., Dupeux, F., Marquez, J. A., et al. (2011). Atomic structure of a nanobody-trapped domain-swapped dimer of an amyloidogenic 2-microglobulin variant. *Proceedings of the National Academy of Sciences*, 108(4), 1314–1319.
- Dreano, M., Brochot, J., Myers, A., Cheng-Meyer, C., Rungger, D., Voellmy, R., et al. (1986). High-level, heat-regulated synthesis of proteins in eukaryotic cells. *Gene*, 49(1), 1–8.
- Elowitz, M. B., & Leibier, S. (2000). A synthetic oscillatory network of transcriptional regulators. *Nature*, 403(6767), 335.
- Filonov, G. S., Piatkevich, K. D., Ting, L. M., Zhang, J., Kim, K., & Verkhusha, V. V. (2011). Bright and stable near-infrared fluorescent protein for in vivo imaging. *Nature Biotechnology*, 29(8), 757.
- Fridy, P. C., Li, Y., Keegan, S., Thompson, M. K., Nudelman, I., Scheid, J. F., et al. (2014). A robust pipeline for rapid production of versatile nanobody repertoires. *Nature Methods*, 11(12), 1253.
- Fu, X., Gao, X., He, S., Huang, D., Zhang, P., Wang, X., et al. (2013). Design and selection of a camelid single-chain antibody yeast two-hybrid library produced de novo for the cap protein of porcine circovirus type 2 (PCV2). *PLoS One*, 8(3), e56222.
- Gerner, E. W., Hersh, E. M., Pennington, M., Tsang, T. C., Harris, D., Vasanwala, F., et al. (2000). Heat-inducible vectors for use in gene therapy. *International Journal of Hyperthermia*, 16(2), 171–181.
- Ghattas, I. R., Sanes, J. R., & Majors, J. E. (1991). The encephalomyocarditis virus internal ribosome entry site allows efficient coexpression of two genes from a recombinant provirus in cultured cells and in embryos. *Molecular and Cellular Biology*, 11(12), 5848–5859.
- Ghosh, E., Kumari, P., Jaiman, D., & Shukla, A. K. (2015). Methodological advances: The unsung heroes of the GPCR structural revolution. *Nature Reviews Molecular Cell Biology*, 16(2), 69.
- Gilon, T., Chomsky, O., & Kulka, R. G. (2000). Degradation signals recognized by the Ubc6p-Ubc7p ubiquitin-conjugating enzyme pair. *Molecular and Cellular Biology*, 20(19), 7214–7219.
- Gossen, M., & Bujard, H. (1992). Tight control of gene expression in mammalian cells by tetracycline-responsive promoters. *Proceedings of the National Academy of Sciences of the United States of America*, 89(12), 5547–5551.

- Greber, D., El-Baba, M. D., & Fussenegger, M. (2008). Intronically encoded siRNAs improve dynamic range of mammalian gene regulation systems and toggle switch. *Nucleic Acids Research*, 36(16), e101.
- Guilliams, T., El-Turk, F., Buell, A. K., O'Day, E. M., Aprile, F. A., Esbjörner, E. K., et al. (2013). Nanobodies raised against monomeric α-synuclein distinguish between fibrils at different maturation stages. *Journal of Molecular Biology*, 425(14), 2397–2411.
- Hillen, W., Gatz, C., Altschmied, L., Schollmeier, K., & Meier, I. (1983). Control of expression of the Tn10-encoded tetracycline resistance genes. Equilibrium and kinetic investigation of the regulatory reactions. *Journal of Molecular Biology*, 169(3), 707–721.
- Holland, A. J., Fachinetti, D., Han, J. S., & Cleveland, D. W. (2012). Inducible, reversible system for the rapid and complete degradation of proteins in mammalian cells. *Proceedings of the National Academy of Sciences of the United States of America*, 109(49), E3350–E3357.
- Hoops, S., Gauges, R., Lee, C., Pahle, J., Simus, N., Singhal, M., et al. (2006). COPASI—A complex pathway simulator. *Bioinformatics*, 22(24), 3067–3074.
- Hornstein, E., & Shomron, N. (2006). Canalization of development by microRNAs. *Nature Genetics*, 38, S20.
- Huang, Q., Hu, J. K., Lohr, F., Zhang, L., Braun, R., Lanzen, J., et al. (2000). Heat-induced gene expression as a novel targeted cancer gene therapy strategy. *Cancer Research*, 60(13), 3435–3439.
- Ingalls, B. P. (2014). Mathematical modelling in systems biology: An introduction. *Journal of Chemical Information and Modeling*, 53(9), 1–396.
- Kisselev, A. F., & Goldberg, A. L. (2001). Proteasome inhibitors: From research tools to drug candidates. *Chemistry and Biology*, 8(8), 739–758.
- Kobayashi, H., Kaern, M., Araki, M., Chung, K., Gardner, T. S., Cantor, C. R., et al. (2004). Programmable cells: Interfacing natural and engineered gene networks. *Proceedings of the National Academy of Sciences of the United States of America*, 101(22), 8414–8419.
- Kolkman, J. A., & Law, D. A. (2010). Nanobodies—From llamas to therapeutic proteins. *Drug Discovery Today: Technologies*, 7(2), e139–e146.
- Korennykh, A. V., Egea, P. F., Korostelev, A. A., Finer-Moore, J., Zhang, C., Shokat, K. M., et al. (2009). The unfolded protein response signals through high-order assembly of Ire1. *Nature*, 457(7230), 687.
- Kracikova, M., Akiri, G., George, A., Sachidanandam, R., & Aaronson, S. A. (2013). A threshold mechanism mediates p53 cell fate decision between growth arrest and apoptosis. *Cell Death and Differentiation*, 20(4), 576.
- Kuhlman, S. J., Quintero, J. E., & McMahon, D. G. (2000). GFP fluorescence reports period1 circadian gene regulation in the mammalian biological clock. *Neuroreport*, 11(7), 1479–1482.
- Li, X., Zhao, X., Fang, Y., Jiang, X., Duong, T., Fan, C., et al. (1998). Generation of destabilized green fluorescent protein as a transcription reporter. *Journal of Biological Chemistry*, 273(52), 34970–34975. https://doi.org/10.1074/jbc.273.52.34970.
- Longo, D., & Hasty, J. (2006). Dynamics of single-cell gene expression. *Molecular Systems Biology*, 2(1), 64.
- MacKeigan, J. P., Murphy, L. O., Dimitri, C. A., & Blenis, J. (2005). Graded mitogenactivated protein kinase activity precedes switch-like c-Fos induction in mammalian cells. *Molecular and Cellular Biology*, 25(11), 4676–4682.
- Mangan, S., & Alon, U. (2003). Structure and function of the feed-forward loop network motif. *Proceedigs of the National Academy of Sciences of the United States of America*, 100(21), 11980–11985.
- March, J. C., Rao, G., & Bentley, W. E. (2003). Biotechnological applications of green fluorescent protein. *Applied Microbiology and Biotechnology*, 62(4), 303–315.

- Mateus, C., & Avery, S. V. (2000). Destabilized green fluorescent protein for monitoring dynamic changes in yeast gene expression with flow cytometry. *Yeast*, 16(14), 1313–1323.
- Matsuzawa, S.-i., Cuddy, M., Fukushima, T., & Reed, J. C. (2005). Method for targeting protein destruction by using a ubiquitin-independent, proteasome-mediated degradation pathway. *Proceedings of the National Academy of Sciences of the United States of America*, 102(42), 14982–14987.
- Monegal, A., Ami, D., Martinelli, C., Huang, H., Aliprandi, M., Capasso, P., et al. (2009). Immunological applications of single-domain llama recombinant antibodies isolated from a naïve library. *Protein Engineering, Design and Selection*, 22(4), 273–280.
- Morikawa, T. J., Fujita, H., Kitamura, A., Horio, T., Yamamoto, J., Kinjo, M., et al. (2016). Dependence of fluorescent protein brightness on protein concentration in solution and enhancement of it. *Scientific Reports*, 6, 22342.
- Moutel, S., Bery, N., Bernard, V., Keller, L., Lemesre, E., De Marco, A., et al. (2016). NaLi-H1: A universal synthetic library of humanized nanobodies providing highly functional antibodies and intrabodies. *eLife*, *5*, e16228.
- Muyldermans, S. (2013). Nanobodies: Natural single-domain antibodies. *Annual Review of Biochemistry*, 82(1), 775–797.
- Nguyen, V. K., Hamers, R., Wyns, L., & Muyldermans, S. (2000). Camel heavy-chain anti-bodies: Diverse germline V(H)H and specific mechanisms enlarge the antigen-binding repertoire. *EMBO Journal*, 19(5), 921–930.
- Nishimura, K., Fukagawa, T., Takisawa, H., Kakimoto, T., & Kanemaki, M. (2009). An auxin-based degron system for the rapid depletion of proteins in nonplant cells. *Nature Methods*, 6(12), 917.
- Olson, E. J., & Tabor, J. J. (2012). Post-translational tools expand the scope of synthetic biology. *Current Opinion in Chemical Biology*, 16(3–4), 300–306.
- Orth, P., Schnappinger, D., Hillen, W., Saenger, W., & Hinrichs, W. (2000). Structural basis of gene regulation by the tetracycline inducible tet repressor-operator system. *Nature Structural Biology*, 7(3), 215–219.
- Pardon, E., Laeremans, T., Triest, S., Rasmussen, S. G. F., Wohlkönig, A., Ruf, A., et al. (2014). A general protocol for the generation of nanobodies for structural biology. *Nature Protocols*, 9(3), 674.
- Patterson, G. H. (2002). A photoactivatable GFP for selective photolabeling of proteins and cells. *Science*, 297(5588), 1873–1877.
- Peng, H.-P., Lee, K. H., Jian, J.-W., & Yang, A.-S. (2014). Origins of specificity and affinity in antibody–protein interactions. *Proceedings of the National Academy of Sciences of the United States of America*, 111(26), E2656–E2665.
- Qin, J. Y., Zhang, L., Clift, K. L., Hulur, I., Xiang, A. P., Ren, B. Z., et al. (2010). Systematic comparison of constitutive promoters and the doxycycline-inducible promoter. *PLoS One*, *5*(5), 3–6.
- Reya, T., Duncan, A. W., Ailles, L., Domen, J., Scherer, D. C., Willert, K., et al. (2003). A role for Wnt signalling in self-renewal of haematopoietic stem cells. *Nature*, 423(6938), 409.
- Sabir, J. S. M., Atef, A., El-Domyati, F. M., Edris, S., Hajrah, N., Alzohairy, A. M., et al. (2014). Construction of naïve camelids VHH repertoire in phage display-based library. *Comptes Rendus Biologies*, 337(4), 244–249.
- Schut, M. H., Pepers, B. A., Klooster, R., van der Maarel, S. M., el Khatabi, M., Verrips, T., et al. (2015). Selection and characterization of llama single domain antibodies against N-terminal huntingtin. *Neurological Sciences*, *36*(3), 429–434.
- Shcherbo, D., Shemiakina, I. I., Ryabova, A. V., Luker, K. E., Schmidt, B. T., Souslova, E. A., et al. (2010). Near-infrared fluorescent proteins. *Nature Methods*, 7(10), 827.

- Slusarczyk, A. L., Lin, A., & Weiss, R. (2012). Foundations for the design and implementation of synthetic genetic circuits. *Nature Reviews Genetics*, 13(6), 406.
- Stearns, T., Prasher, D., Tsien, R., Ward, W., & Prasher, D. (1995). Green fluorescent protein. The green revolution. *Current Biology: CB*, 5(3), 262–264.
- Takeda, K., Shao, D., Adler, M., Charest, P. G., Loomis, W. F., Levine, H., et al. (2012). Cell biology: Incoherent feedforward control governs adaptation of activated ras in a eukaryotic chemotaxis pathway. *Science Signaling*, 5(205), 29–31.
- Tigges, M., Marquez-Lago, T. T., Stelling, J., & Fussenegger, M. (2009). A tunable synthetic mammalian oscillator. *Nature*, 457(7227), 309.
- Tsien, R. Y. (1998). The green fluorescent protein. *Annual Review of Biochemistry*, 67(1), 509–544.
- Van Der Linden, R. H. J., Frenken, L. G. J., De Geus, B., Harmsen, M. M., Ruuls, R. C., Stok, W., et al. (1999). Comparison of physical chemical properties of llama VHH antibody fragments and mouse monoclonal antibodies. *Biochimica et Biophysica Acta (BBA)-*Protein Structure and Molecular Enzymology, 1431(1), 37–46.
- Verkhusha, V. V., Kuznetsova, I. M., Stepanenko, O. V., Zaraisky, A. G., Shavlovsky, M. M., Turoverov, K. K., et al. (2003). High stability of discosoma DsRed as compared to aequorea EGFP. *Biochemistry*, 42(26), 7879–7884.
- Villaverde, A. F., & Banga, J. R. (2014). Reverse engineering and identification in systems biology: Strategies, perspectives and challenges. *Journal of the Royal Society Interface*, 11(91), 1–16.
- Wu, B. J., Kingston, R. E., & Morimoto, R. I. (1986). Human HSP70 promoter contains at least two distinct regulatory domains. *Proceedings of the National Academy of Sciences of the United States of America*, 83(3), 629–633.
- Yan, J., Li, G., Hu, Y., Ou, W., & Wan, Y. (2014). Construction of a synthetic phage-displayed nanobody library with CDR3 regions randomized by trinucleotide cassettes for diagnostic applications. *Journal of Translational Medicine*, 12(1), 343.
- Yao, F., Svensjö, T., Winkler, T., Lu, M., Eriksson, C., & Eriksson, E. (1998). Tetracycline repressor, tetR, rather than the cell transcription factor fusion derivatives, regulates inducible gene expression in mammalian cells. *Human Gene Therapy*, 1950, 1939–1950.
- Yau, R., & Rape, M. (2016). The increasing complexity of the ubiquitin code. *Nature Cell Biology*, 18(6), 579.
- Zhao, W., Bonem, M., McWhite, C., Silberg, J. J., & Segatori, L. (2014). Sensitive detection of proteasomal activation using the Deg-On mammalian synthetic gene circuit. *Nature Communications*, 5, 1–12.
- Zhao, W., Pferdehirt, L., & Segatori, L. (2018). Quantitatively predictable control of cellular protein levels through proteasomal degradation. *ACS Synthetic Biology*, 7(2), 540–552.
- Zi, Z. (2011). Sensitivity analysis approaches applied to systems biology models. *IET Systems Biology*, *5*(6), 336–346.